

RESEARCH LETTER

10.1002/2017GL073227

Key Points:

- A century-long reconstructed South Atlantic Meridional Overturning Circulation index from sea surface temperature is presented
- The Interdecadal Pacific Oscillation and Atlantic Niño are the main contributors of interannual/decadal covariability of SST and SAMOC
- SAMOC is currently in an anomalous positive phase

Supporting Information:

- Supporting Information S1

Correspondence to:

H. Lopez
hlopez@rsmas.miami.edu

Citation:

Lopez, H., G. Goni, and S. Dong (2017), A reconstructed South Atlantic Meridional Overturning Circulation time series since 1870, *Geophys. Res. Lett.*, *44*, 3309–3318, doi:10.1002/2017GL073227.

Received 24 FEB 2017

Accepted 27 MAR 2017

Accepted article online 30 MAR 2017

Published online 14 APR 2017

©2017. The Authors.

This is an open access article under the terms of the Creative Commons Attribution-NonCommercial-NoDerivs License, which permits use and distribution in any medium, provided the original work is properly cited, the use is non-commercial and no modifications or adaptations are made.

A reconstructed South Atlantic Meridional Overturning Circulation time series since 1870

Hosmay Lopez^{1,2} , Gustavo Goni², and Shenfu Dong² 

¹Cooperative Institute for Marine and Atmospheric Studies, University of Miami, Miami, Florida, USA, ²Atlantic Oceanographic and Meteorological Laboratory, NOAA, Miami, Florida, USA

Abstract This study reconstructs a century-long South Atlantic Meridional Overturning Circulation (SAMOC) index. The reconstruction is possible due to its covariability with sea surface temperature (SST). A singular value decomposition (SVD) method is applied to the correlation matrix of SST and SAMOC. The SVD is performed on the trained period (1993 to present) for which Expendable Bathythermographs and satellite altimetry observations are available. The joint modes obtained are used in the reconstruction of a monthly SAMOC time series from 1870 to present. The reconstructed index is highly correlated to the observational based SAMOC time series during the trained period and provides a long historical estimate. It is shown that the Interdecadal Pacific Oscillation (IPO) is the leading mode of SAMOC-SST covariability, explaining ~85% with the Atlantic Niño accounting for less than 10%. The reconstruction shows that SAMOC has recently shifted to an anomalous positive period, consistent with a recent positive shift of the IPO.

1. Introduction

There is currently limited knowledge about the underlying mechanisms that govern the South Atlantic Meridional Overturning Circulation (SAMOC) variability and how it might feedback into climate, partly due to the small number of direct observations in this ocean basin. Observational estimates of the SAMOC can be obtained from the beginning of the satellite altimetry period, which started in 1993 [Dong *et al.*, 2015]. Direct observations have been confined mostly to a latitudinal transect at 34.5°S. These observations are carried out using different observing platforms; for example, High Density Expendable Bathythermographs (XBT) since 2002 [Dong *et al.*, 2009; Garzoli *et al.*, 2013], Argo float measurements [Dong *et al.*, 2011, Majumder *et al.*, 2016], and boundary array of inverted echo sounders since 2009 [Meinen *et al.*, 2013]. The longest nonsatellite observational record of the SAMOC corresponds to the time series obtained from one XBT transect since 2002, namely, AX18, which runs from Buenos Aires, Argentina, to Cape Town, South Africa. Motivated by the limited availability of the SAMOC observations, Dong *et al.* [2015] estimated the volume and heat transport in the South Atlantic using satellite altimetry and a suite of in situ measurements. In that study, they found that altimetry observations could be used to derive the SAMOC, allowing the creation of an extended observational record that starts in 1993. These estimates can be obtained given the correspondence that exists between the sea surface height and the underlying ocean temperatures, mainly below the main thermocline depth [Goni *et al.*, 1996, 2011; Mayer *et al.*, 2001]. In this study, the contribution of the geostrophic and Ekman components to the total SAMOC was found to vary with time scales of 10 years or longer at different latitudes. In a similar study, Majumder *et al.* [2016] used Argo profiling float and satellite altimetry observations to derive three-dimensional velocity profiles to estimate volume and heat transport in the South Atlantic for the period of 2000–2014 and found strong correlations between the strength of SAMOC and meridional heat transport (MHT) at 35°S, 30°S, 25°S, and 20°S.

Although the altimetry-derived SAMOC time series provides a relatively long record, decadal and multidecadal variability of the SAMOC and its influence on climate and weather cannot be assessed due to its short temporal record. Given this, most of the current understanding of the SAMOC, and its governing mechanism, depends on the use of numerical models [e.g., Stouffer *et al.*, 2006; Smith and Gregory, 2009; Sitz *et al.*, 2015]. The SAMOC derived from climate models has led to several hypotheses for the mechanism governing SAMOC variability. For example, Biastoch *et al.* [2009] and Lee *et al.* [2011] suggested that interocean transport from the Indian into the Atlantic Ocean could be a potential source of the anomalous SAMOC variability. Yeager and Danabasoglu [2014] found that most of the SAMOC variability is accounted by changes in the Southern Ocean westerlies, although other studies showed that the influence of Southern Hemisphere

wind stress onto the SAMOC depends on model representation of mesoscale eddies [Farneti and Delworth, 2010]. In addition, model bias in the representation of the Southern Hemisphere wind stress field makes it difficult to understand the correct response of SAMOC to wind stress changes.

A recent study by Lopez *et al.* [2016a] found that low-frequency variability of MHT in the South Atlantic Ocean associated with changes in the SAMOC could influence monsoon rainfall. They argue that a weaker than normal SAMOC forces an interhemispheric Hadley circulation, transporting anomalous atmospheric heat from the Northern Hemisphere (NH) to the Southern Hemisphere (SH) and moisture from the SH to the NH, thereby modulating global monsoons. The opposite holds for the case of positive SAMOC anomalies.

This result serves as a motivation to reconstruct the SAMOC from a longer and more readily available data set, namely, sea surface temperature (SST), which can be used to monitor the state of the SAMOC and its impact on climate and weather. Our hypothesis is that the SAMOC and modes of SST variability in the South Atlantic are correlated. The reconstruction is based on the statistical relationship between the SAMOC time series and SST field obtained during the observed (i.e., trained) period (1993 to present). There are multiple SST products available since the mid-1800s, although there are potential shortcomings with the SST records, especially for the earlier periods. Therefore, we will use several SST products to validate the results. This manuscript is organized as follows. The data sets and methodology are described in section 2. Section 3 discusses the SAMOC reconstruction from SST. Potential climate factors influencing the covariability between SAMOC and SST in the South Atlantic are presented in section 4. The summary and discussion are presented in section 5.

2. Data Sets and Methodology

The SAMOC data used in this study are the time series derived from XBT and satellite altimetry at 34°S, 30°S, 25°S, and 20°S latitudes for the period of 1993–2015 [Dong *et al.*, 2015]. These are currently the longest observational based SAMOC estimates available. Four SST products are employed, including the Hadley Centre SST (HadSST), the Extended Reconstructed SST versions 3 and 4 (ERSSTv3 and ERSSTv4), and the Centennial Observational Based Estimates SST (COBE-SST) [Reynolds *et al.*, 2002; Parker *et al.*, 1994; Smith *et al.*, 1996; Kaplan *et al.*, 1998; Ishii *et al.*, 2005]. Readers are referred to Huang *et al.* [2015] for a thorough description of the strength/weakness of these SST reanalysis products.

The use of multiple products brings two benefits. First, the comparison among reconstructions during the trained period (i.e., 1993 to present) with the actual XBT-altimetry-derived SAMOC will allow to assess each SST product. Second, the comparison among reconstructions during the untrained period (i.e., before 1993) should allow quantifying the fidelity of the reconstruction, especially prior to the satellite era.

SVD analysis is used to find coupled patterns of variability between two fields. For example, two data vectors denoted $\mathbf{x}(t)$ (i.e., SST herein), which covers p stations or grid points over m temporal records and $\mathbf{y}(t)$ (i.e., SAMOC herein), which covers q stations over n temporal records, are evaluated here. Thus, \mathbf{x} is a $(p \times m)$ matrix and \mathbf{y} is a $(q \times n)$ matrix. An SVD analysis (1) on the cross-covariance or correlation matrix C_{xy} of \mathbf{x} and \mathbf{y} can be performed. Note that C_{xy} is a $(p \times q)$ matrix.

$$C_{xy} = \mathbf{U}\mathbf{\Sigma}\mathbf{V}^T \quad (1)$$

From (1), \mathbf{U} is a $(p \times m)$ matrix, whose columns contain the singular vectors of \mathbf{x} , or the left field here onward. \mathbf{V}^T is a $(n \times q)$ matrix, which rows contain the singular vectors of \mathbf{y} , or the right field. The matrix $\mathbf{\Sigma}$ has dimensions of $(m \times n)$, which diagonal entries are the squared covariance factors or eigenvalues. Each pair of singular vectors (\mathbf{U}_k , \mathbf{V}_k) corresponds to a singular eigenvalue. Given this, sets of expansion coefficients can be obtained by projecting the singular vectors to their respective data matrix ((2a) and (2b)):

$$a_k(t) = \mathbf{U}_k^T \mathbf{x}(t) \quad (2a)$$

$$b_k(t) = \mathbf{V}_k^T \mathbf{y}(t) \quad (2b)$$

The temporal expansion coefficient for the left and right fields, a_k and b_k respectively, are of key value in describing the covariability between the data vectors \mathbf{x} and \mathbf{y} [Bretherton *et al.*, 1992]. For example, one

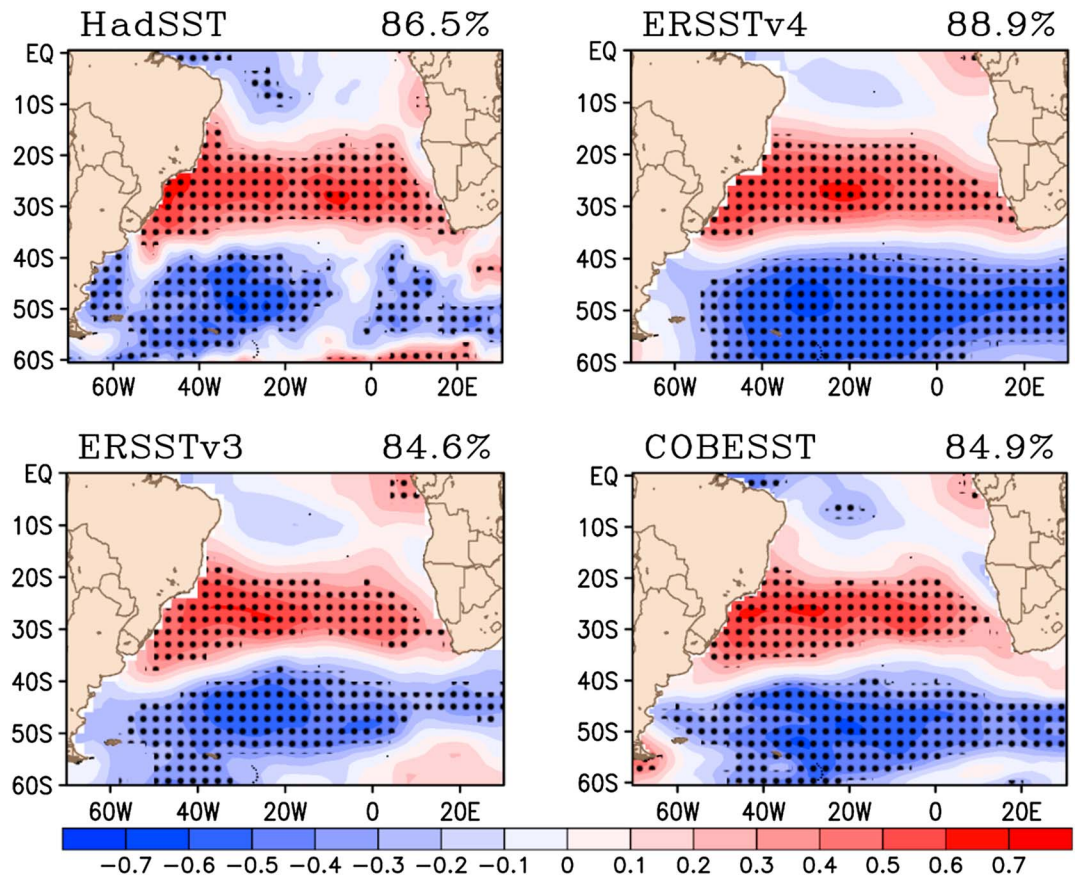


Figure 1. Heterogeneous correlation for the first joint singular vector from the observed SAMOC SST covariance matrix for each SST product. Black hatching indicates where the heterogeneous correlation is significant at a 95% confidence level. The percentage on the top right indicates the amount of covariance explained by the first mode.

can project the expansion coefficient from one field into the data vector of the other to produce heterogeneous correlation maps, $r_{het}[b_k(t), \mathbf{x}(t)]$ and $r_{het}[a_k(t), \mathbf{y}(t)]$. The heterogeneous correlation map is useful to assess how well one field can be predicted from the knowledge of the state of the other field.

The methodology described above is used to perform SVD between the altimetry-derived SAMOC and SST in the South Atlantic for the period 1993 to present. First, we detrend both data sets. This is done to filter long-term climate trends, as we are mainly assessing the internal variability. Interannual anomalies are obtained by removing the monthly climatology. A 13 month running average is also applied to each data vector. Lastly, the data vectors are normalized by their respective standard deviation in order to perform the SVD analysis on the correlation matrix of SST and SAMOC.

We will use the SVD patterns obtained for the 1993 to present trained period to reconstruct the SAMOC for the untrained period 1870 to present, which starts prior to the altimetry era constrained by the longer observed SST field (3). The reconstructed SAMOC time series $\hat{y}(t)$ is readily obtained from the SST data vector $x(t)$, where t indicates the time index (e.g., monthly variant). Note that the relative strength of each mode is measured by the ratio of covariance and variance of each expansion coefficient. The reconstruction is limited by the smaller number of station data of the SAMOC vector (i.e., $q = 4$ corresponding to 20°S, 25°S, 30°S, and 34°S). Thus, we can obtain a time series for each of these latitude points such that \hat{y} is a function of latitude and time.

$$\hat{y}(t) = \sum_{k=1}^q \frac{\text{cov}(a_k, b_k)}{\text{var}(a_k)} \mathbf{U}_k^T \mathbf{x}(t) \mathbf{V}_k, \quad q = 4, \quad t = 1870 : 2015 \quad (3)$$

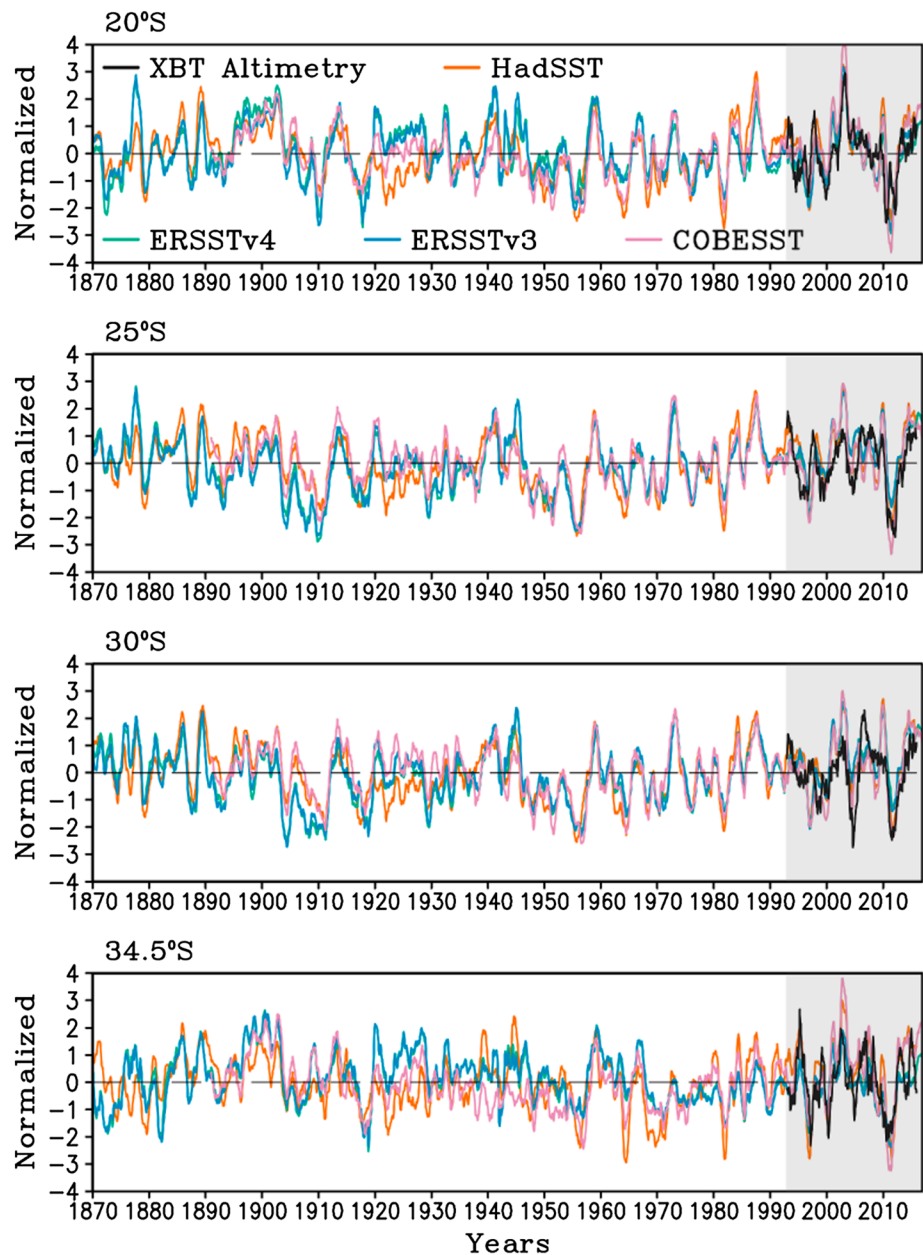


Figure 2. SAMOC time series obtained from altimetry (black) and those reconstructed from SST and SAMOC joint variability (color). All time series were normalized by their standard deviation. The trained period is highlighted by a grey box.

3. SAMOC Reconstruction

Figure 1 shows the heterogeneous correlation for the first joint SVD vectors from the observed SAMOC and the four SST products. Black stipples indicate where correlations are significant at 95% confidence levels. It is important to note that the leading mode explains >84% of the joint variability between SST and the SAMOC independent of the SST product used. The heterogeneous correlations resemble a meridional dipole pattern centered in the South Atlantic Subtropical Gyre. This result is consistent with Lopez *et al.* [2016b], who found that low-frequency variability of the SAMOC is tightly associated with the leading mode of variability of sea surface height in the South Atlantic Ocean.

The second joint pattern explains <10% of the joint covariance and shows a positive loading near the South American coast and a dominant negative loading in the equatorial Atlantic, which extends into the Benguela

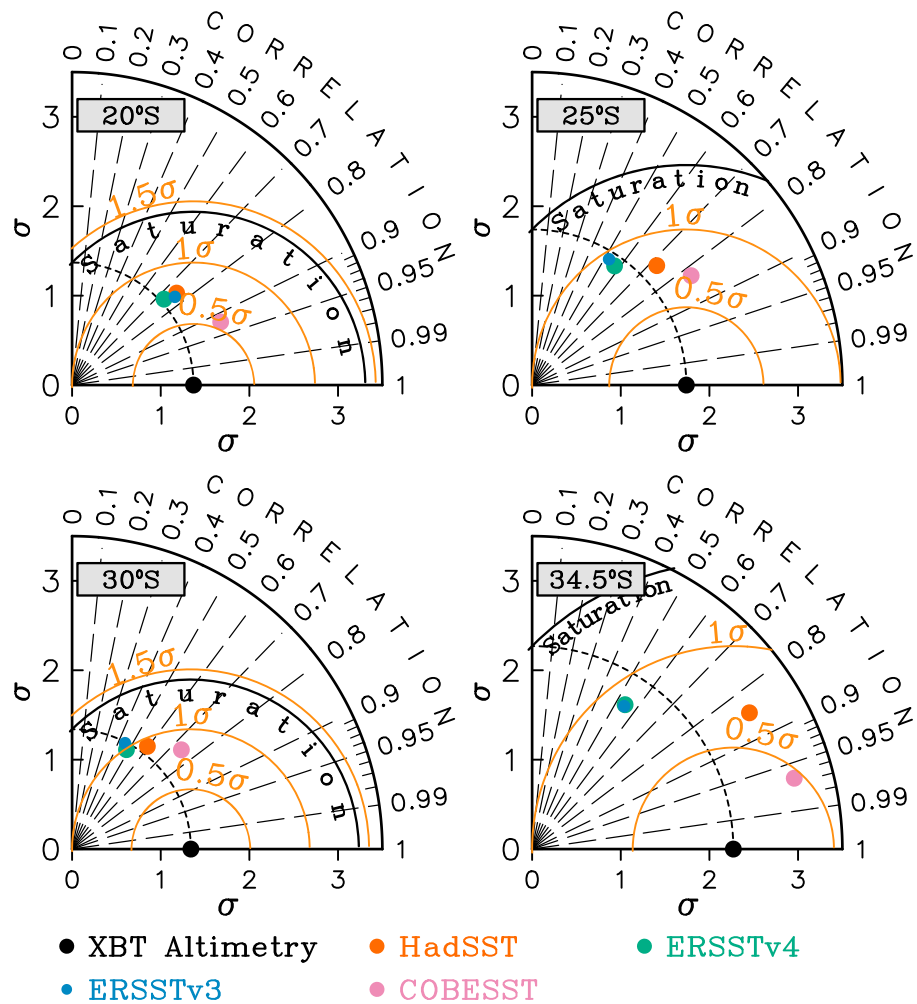


Figure 3. Taylor diagram for the reconstruction of the MOC using different SST products with respect to the observed XBT-altimetry-derived MOC (black dot). Note that the radial axes describe standard deviation (σ) in sverdrup and the azimuthal axis indicates correlation. The concentric orange circles with respect to the observed MOC indicate root-mean-square error (RMSE) in standard deviation units. That is, the closer a point is to the observed MOC, the better the reconstruction. The RMSE for all reconstructions are significantly smaller than the saturation RMSE (RMSE equal to $\sqrt{2}\sigma$) shown by black semicircle.

current region (Figure S1 in the supporting information). Most of the variability associated with the third pattern is found near the Brazil-Malvinas Confluence region (Figure S2), explaining less than 7% of the joint variability between SAMOC and SST. The last pattern (Figure S3) explains $<1\%$ of the covariability.

The patterns described in Figures 1 and S1–S3 are used here, as stated in (3) to reconstruct the SAMOC time series from each SST product. The reconstructed monthly mean SAMOC anomalies are shown in Figure 2 extending back to 1870. Note that the reconstructed SAMOC and the altimetry-derived SAMOC are very well correlated from 1993 to present for all latitudes. This is described in Figure 3, which shows a Taylor diagram as deterministic skill measure of the goodness of fit between the observed and reconstructed SAMOC time series for the trained period for all latitudes and all SST products. The root-mean-square error (RMSE) of the reconstructed time series is considerably smaller than the saturation RMSE error for all cases, indicating that errors in the reconstruction are much smaller than the observed SAMOC variability. There are some marked differences in the quality of the reconstruction regarding latitude and SST product used. For example, ERSSTv3 and ERSSTv4 show the lowest correlation (e.g., $0.5 < r < 0.78$ depending on latitude) but the most accurate standard deviation (σ) with respect to (w.r.t.) the observed σ as depicted by the azimuthal dashed line. The reconstruction using the COBE-SST presents the smallest RMSE and highest correlation w.r.t. the

observed (e.g., $0.74 < r < 0.97$ depending on latitude), although its σ is consistently larger than that of the observed. The HadSST reconstruction systematically lies between the COBE-SST and both ERSST products (e.g., $0.6 < r < 0.85$ depending on latitude).

This high degree of agreement is indicative of a statistical correspondence between SST and SAMOC and such correspondence is well modeled by the statistical method used here. It also provides great degree of accuracy of the reconstruction prior to the observation record. The reconstructions are very similar among SST products during the untrained period (Figure S4) with the correlations exceeding 0.9 for the 20°S, 25°S, and 30°S and 0.7 for the 34.5°S. The large agreement among the SAMOC indices during the untrained period adds confidence to the reconstruction. The reconstruction of the SAMOC obtained here provides valuable information that is impossible to obtain from the current observational records alone. For example, results show that there is considerable interannual variability imbedded into large multidecadal variations in the SAMOC for all four latitudes (see supporting information Figures S5–S8). The SAMOC interannual variability in the South Atlantic is highly dependent on latitude. Wavelet analysis suggests that the volume transport at 20°S and 25°S are currently stronger than normal in a multidecadal sense, whereas the transport at 30°S and 34°S indicates a shift from neutral to a positive (anomalous northward) phase (supporting information). Since the SVD analysis was trained using a detrended SST and SAMOC data, this notion of weakening/strengthening SAMOC is due to internal variability, and not to be misunderstood with those associated with slowdown due to climate change.

4. Factors Influencing SAMOC-SST Covariability

We investigate climate factors influencing SAMOC-SST covariability. Lopez *et al.* [2016b] showed that diabatic heating from the Interdecadal Pacific Oscillation (IPO) forces atmospheric teleconnection patterns, which eventually influence the wind stress fields over the South Atlantic modulating the SAMOC. Motivated by this, we use the expansion coefficient reconstructed in (2a) for the first two modes, which accounts for more than 90% of the covariability between the SST and the SAMOC. Figure 4 shows the normalized monthly mean expansion coefficient of the first two SST modes (e.g., a_1 and a_2) and the normalized IPO and Atlantic Niño indices. The spatial correlations of interannual SST anomalies with these indices are also shown.

The IPO is multidecadal SST variability in the Pacific, different from El Niño–Southern Oscillation. It shows a symmetric structure about the equator very similar in the North Pacific to the Pacific Decadal Oscillation described by Mantua *et al.* [1997]. The IPO is known to modulate the strength of the South Pacific Convergence Zone [Folland *et al.*, 2002]. It is worth noting the similarity between the IPO and the leading mode that explains about 85% of the SST-SAMOC covariability. This is consistent with the relationship of the IPO and the SAMOC [Lopez *et al.*, 2016b].

The spatial pattern associated with mode 2 is a dipole in SST with a loading over the tropical Eastern Atlantic and a pole of opposite sign over the southwestern subtropical South Atlantic (Figure 4d), which is similar to the so-called Atlantic Niño [Zebiak, 1993; Keenlyside and Latif, 2007] shown in Figure 3f. The expansion coefficient a_2 in Figure 4b is multiplied by minus one for easy comparison with the Atlantic Niño index. These two indices show large anticorrelation ($r = -0.92$) in their temporal variability as well as their correlation with global SST anomalies.

The Atlantic Niño is the equivalent to the Pacific Niño but peaks during the boreal summer [Zebiak, 1993; Keenlyside and Latif, 2007]. A positive Atlantic Niño is characterized by warm SST anomalies over the tropical eastern Atlantic. While this mode of SST variability has been widely studied, the underlying mechanisms are still not well understood. One view is that ocean dynamics may be a key factor in the growth of the Atlantic El Niño through positive Bjerknes feedback mechanism [Zebiak, 1993; Ding *et al.*, 2010; Hu *et al.*, 2013], equatorial Kelvin waves [Brandt *et al.*, 2011], or meridional temperature advection [Richter *et al.*, 2013]. A competing view is that ocean dynamics only plays a minor role and that atmospheric stochastic forcing is responsible for the growth of tropical Atlantic SST anomalies [Trzaska *et al.*, 2007; Wang and Chang, 2008].

The meridional SST structures associated with the Atlantic Niño (Figures 4d and 4f) are similar to the so-called South Atlantic Subtropical Dipole (SASD) [Venegas *et al.*, 1997; Haarsma *et al.*, 2005; Morioka *et al.*, 2011]. There is still debate whether the Atlantic Niño and the SASD are part of the same mode or independent from each other. For example, Nnamchi *et al.* [2011] argued that these two modes are independent. On the other hand

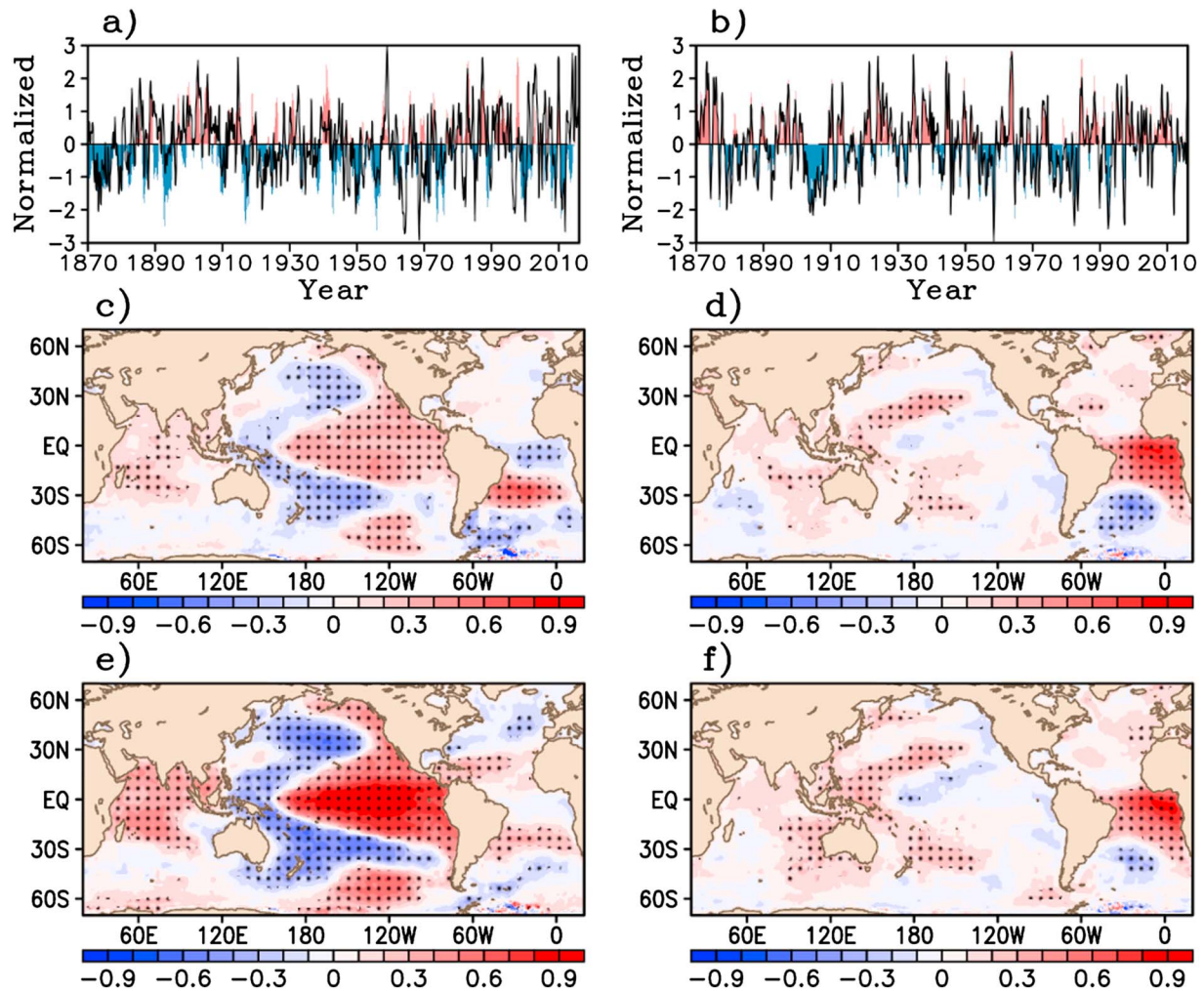


Figure 4. (a) Normalized expansion coefficient (a_1 from equation (2a)) for the first mode of SST and SAMOC variability (black) and the normalized Interdecadal Pacific Oscillation Index, IPO (color). Both time series are smoothed by a 3 month running average. (b) Same as Figure 4a but for the normalized (negative) expansion coefficient (a_2 from equation (2a)) for the second mode of SST and SAMOC variability (black) and the normalized Atlantic Niño Index (color). (c–f) The correlation between SST anomaly and a_1 , negative a_2 , IPO index, and Atlantic Niño index. Hatching indicates regions of significant correlation at a 95% confidence level.

in a separate study, the same author demonstrated that the Atlantic Niño can be viewed as the equatorial branch of the SASD and that the southern pole of the SASD is significantly anticorrelated with the Atlantic Niño [Nnamchi et al., 2016]. Regardless of the origin of the Atlantic Niño or whether it is independent of the SASD, the Atlantic Niño appears to play a secondary role to the IPO in terms of the SST-SAMOC variability. The variance explained by this mode is much smaller than that associated with the IPO. Overall, the IPO [Lopez et al., 2016b] dominates with covariance explained higher than 85% for all SST products.

5. Discussion

Using a reconstructed AMOC time series in the South Atlantic, it was shown that while decadal variability of the SAMOC is coherent at 20°S and 25°S, there are larger differences with respect to those at 30°S and 34°S. There is also considerable differences in the interannual variability. Figure 5 shows the linear projection between the reconstructed SAMOC at different latitudes (labeled colored axes) and the first two SST expansion coefficients a_1 (horizontal axis) and a_2 (vertical axis) for the period of 1870–2015. Recall that a_1 is explained by the IPO and a_2 is explained by the negative Atlantic Niño. The variability of the SAMOC at 30°S is mostly explained by the first SST expansion coefficient (e.g., the red axis is parallel to the horizontal

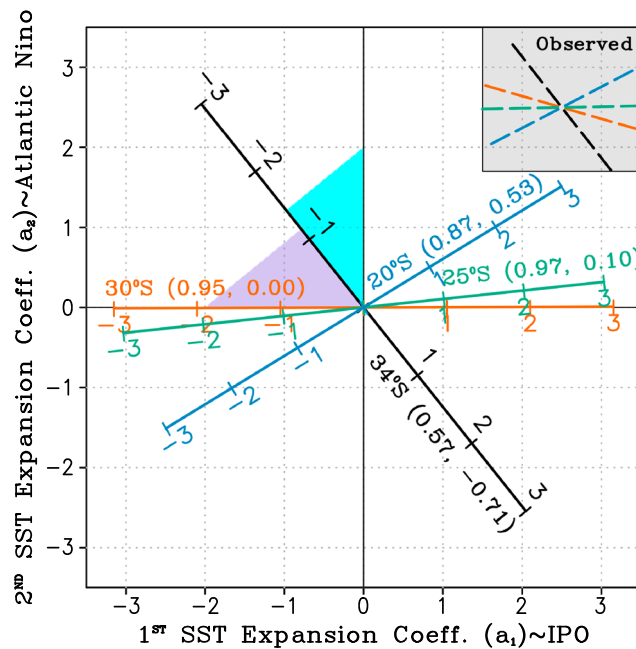


Figure 5. Linear projection between the reconstructed SAMOC at different latitudes (labeled colored axes) and the first two SST expansion coefficients a_1 (horizontal axis) and a_2 (vertical axis). The projection between any two axes indicates their correlation. Note that a_1 and a_2 are orthogonal. For illustration purpose, the purple (aqua) triangle indicates the projection between a_1 (a_2) and the AMOC at 34°S. The gray rectangle in the upper right serves to illustrate that the relationship between first two SST expansion coefficients and the observed AMOC at different latitudes is similar.

axis with correlation of 0.95 for a_1 and 0 for a_2). Similarly, the SAMOC at 25°S has a correlation of 0.97 for a_1 and 0.10 for a_2 . Also, the SAMOC at 20°S is significantly correlated with a_1 (0.87) and a_2 (0.53). Note that the SAMOC at 34°S is significantly correlated with both expansion coefficients, although it has a negative relation to mode 2. In summary, the SAMOC is positively correlated with the IPO at all four latitudes. In contrast, the relationship of SAMOC and the Atlantic Niño is dependent on latitude, with positive correlation with SAMOC at 20°S, negative correlation at 34°S, and little correlation at 25°S and 30°S.

It is important to note that the SAMOC at 34°S is nearly orthogonal to the SAMOC at 20°S. This is true from the reconstructed (e.g., correlation $r = 0.18$) as well as from the observed (correlation $r = 0.19$) period, which advocates for the implementation of observing systems at different latitudes. This finding is consistent with *Dong et al.* [2015], which found that the correlation of SAMOC at 34°S with all other three latitudes discussed here were below the 95% significant level. In that study, they hypothesized potential factors influencing these low correlations, including the Brazil and Benguela Currents and the Agulhas leakage, although their relative short temporal record limited further assessments for identifying drivers of meridionally asymmetric SAMOC behavior.

The latitudinal coherence (e.g., meridional structure) of the reconstructed SAMOC is very similar to the observed SAMOC given that their correlation differences do not pass a significance test at 95% confidence level for any latitude pair (See Table S1 in the supporting information). So we can reject the null hypothesis and confirm that the meridional coherence is similar between the observed and reconstructed SAMOC. These results are consistent with those shown in Figure 5, adding fidelity to the reconstruction.

The high degree of accuracy of the reconstruction presented here may allow for more comprehensive studies on SAMOC variability and potential influence on climate and weather to carry out additional research on the impact of the South Atlantic on global climate and extreme weather events, similar to *Lopez et al.* [2016a]. Future work on this topic will include the assessment of physical mechanism driving the distinction between the SAMOC at 34°S and elsewhere and the latitudinal symmetric (asymmetric) relationship with the IPO (Atlantic Niño). *Dong et al.* [2015] also pointed out that the relative influence of the Ekman and geostrophic components varies on interannual timescales. This nonstationary behavior could be investigated using the reconstructed data sets presented here. Multidecadal variability of the SAMOC and its influence on extreme weather will also be investigated in future studies, partially motivated by the findings of *Lopez et al.* [2016a].

The statistical reconstruction shows that SAMOC is currently in an anomalous positive (i.e., stronger than normal) phase. Concurrently, the IPO has recently shifted to a positive phase [*Burgman et al.*, 2017]. Given this, and according to the mechanism presented in *Lopez et al.* [2016b], anomalous tropical Pacific convection associated with the positive phase of the IPO forces robust stationary Rossby wave patterns, modulating the wind stress curl over the South Atlantic Ocean. This in turn increases the westerlies over the South

Atlantic, which intensifies the strength of the Subtropical Gyre in the South Atlantic and thus the SAMOC. This physical mechanism aligns with the results presented here and the current state of the SAMOC.

To conclude, it is worth noting that the reconstruction presented here is not a replacement of the current observing systems. In fact, it is a testament of the effort in sustaining several key ocean observational platforms, such as XBTs and Argo floats, and the importance of their joint analysis with satellite altimetry observations, which allowed for studies such as the one presented here to be carried out.

Acknowledgments

This research was carried out in part under the auspices of the Cooperative Institute of Marine and Atmospheric Studies, a cooperative institute of the University of Miami, and the National Oceanic and Atmospheric Administration (NOAA), cooperative agreement NA10OAR4320143. This work was funded by NOAA Atlantic Oceanographic and Meteorological Laboratory and by the Climate Observations Division of the NOAA Climate Program Office. S.D. is also partially supported by NASA grant NN H13AW331. MOC time series data can be obtained upon request by contacting the corresponding author at hlopez@rsmas.miami.edu.

References

- Biastoch, A., C. W. Böning, F. U. Schwarzkopf, and J. Lutjeharms (2009), Increase in Agulhas leakage due to poleward shift of Southern Hemisphere westerlies, *Nature*, *462*(7272), 495–498.
- Brandt, P., A. Funk, V. Hormann, M. Dengler, R. J. Greatbatch, and J. M. Toole (2011), Interannual atmospheric variability forced by the deep equatorial Atlantic Ocean, *Nature*, *473*(7348), 497–500, doi:10.1038/nature10013.
- Bretherton, C. S., C. Smith, and J. M. Wallace (1992), An intercomparison of methods for finding coupled patterns in climate data, *J. Clim.*, *5*, 541–560.
- Burgman, R. J., B. P. Kirtman, A. C. Clement, and H. Vazquez (2017), Model evidence for low-level cloud feedback driving persistent changes in atmospheric circulation and regional hydroclimate, *Geophys. Res. Lett.*, *44*, 428–437, doi:10.1002/2016GL071978.
- Ding, H., N. Keenlyside, and M. Latif (2010), Equatorial Atlantic interannual variability: The role of heat content, *J. Geophys. Res.*, *115*, C09020, doi:10.1029/2010JC006304.
- Dong, S., S. Garzoli, M. Baringer, C. Meinen, and G. Goni (2009), Interannual variations in the Atlantic meridional overturning circulation and its relationship with the net northward heat transport in the South Atlantic, *Geophys. Res. Lett.*, *36*, L20606, doi:10.1029/2009GL039356.
- Dong, S., M. Baringer, G. Goni, and S. Garzoli (2011), Importance of the assimilation of Argo float measurements on the Meridional Overturning Circulation in the South Atlantic, *Geophys. Res. Lett.*, *38*, L18603, doi:10.1029/2011GL048982.
- Dong, S., G. Goni, and F. Bringas (2015), Temporal variability of the Meridional Overturning Circulation in the South Atlantic between 20°S and 35°S, *Geophys. Res. Lett.*, *42*, 7655–7662, doi:10.1002/2015GL065603.
- Farneti, R., and T. L. Delworth (2010), The role of mesoscale eddies in the remote oceanic response to altered Southern Hemisphere winds, *J. Phys. Oceanogr.*, *40*, 2348–2354, doi:10.1175/2010JPO4480.1.
- Folland, C. K., J. A. Renwick, M. J. Salinger and A. B. Mullan (2002), Relative influences of the Interdecadal Pacific Oscillation and ENSO on the South Pacific Convergence Zone, *Geophys. Res. Lett.*, *29*(13), 1643, doi:10.1029/2001GL014201.
- Garzoli, S. L., M. O. Baringer, S. Dong, R. C. Perez, and Q. Yao (2013), South Atlantic meridional fluxes, *Deep-Sea Res. I Oceanogr. Res. Pap.*, *71*, 21–32, doi:10.1016/j.dsr.2012.09.003.
- Goni, G., S. Kamholz, S. Garzoli, and D. Olson (1996), Dynamics of the Brazil-Malvinas Confluence based on inverted echo sounders and altimetry, *J. Geophys. Res.*, *101*(C7), 16,273–16,289, doi:10.1029/96JC01146.
- Goni, G. J., F. Bringas, and P. N. DiNezio (2011), Observed low frequency variability of the Brazil current front, *J. Geophys. Res.*, *116*, C10037, doi:10.1029/2011JC007198.
- Haarsma, R. J., E. J. D. Campos, W. Hazeleger, C. Severijns, A. R. Piola, and F. Molteni (2005), Dominant modes of variability in the South Atlantic: A study with a hierarchy of ocean-atmosphere models, *J. Clim.*, *18*, 1719–1735, doi:10.1175/JCLI3370.1.
- Hu, Z.-Z., A. Kumar, B. Huang, and J. Zhu (2013), Leading modes of the upper-ocean temperature interannual variability along the equatorial Atlantic Ocean in NCEP GODAS, *J. Clim.*, *26*(13), 4649–4663, doi:10.1175/JCLI-D-12-00629.1.
- Huang, B., et al. (2015), Extended reconstructed sea surface temperature version 4 (ERSST.v4). Part I: Upgrades and intercomparisons, *J. Clim.*, *28*(3), 911–930.
- Ishii, M., A. Shouji, S. Sugimoto, and T. Matsumoto (2005), Objective analyses of sea-surface temperature and marine meteorological variables for the 20th century using ICOADS and the Kobe collection, *Int. J. Climatol.*, *25*(7), 865–879.
- Kaplan, A., M. A. Cane, Y. Kushnir, A. C. Clement, M. B. Blumenthal, and B. Rajagopalan, (1998), Analyses of global sea surface temperature 1856–1991, *J. Geophys. Res.*, *103*(C9), 18,567–18,589.
- Keenlyside, N., and M. Latif (2007), Understanding equatorial Atlantic interannual variability, *J. Clim.*, *20*(1), 131–142, doi:10.1175/JCLI3992.1.
- Lee, S. K., W. Park, E. van Sebille, M. O. Baringer, C. Wang, D. B. Enfield, S. G. Yeager, and B. P. Kirtman (2011), What caused the significant increase in Atlantic Ocean heat content since the mid-20th century?, *Geophys. Res. Lett.*, *38*, L17607, doi:10.1029/2011GL048856.
- Lopez, H., S. Dong, S.-K. Lee, and G. Goni (2016a), Decadal modulations of interhemispheric global atmospheric circulations and monsoons by the South Atlantic Meridional Overturning Circulation, *J. Clim.*, *29*, 1831–1851, doi:10.1175/JCLI-D-15-0491.1.
- Lopez, H., S. Dong, S.-K. Lee, and E. Campos (2016b), Remote influence of Interdecadal Pacific oscillation on the South Atlantic meridional overturning circulation variability, *Geophys. Res. Lett.*, *43*, 8250–8258, doi:10.1002/2016GL069067.
- Majumder, S., C. Schmid, and G. Halliwell (2016), An observations and model-based analysis of meridional transports in the South Atlantic, *J. Geophys. Res. Oceans*, *121*, 5622–5638, doi:10.1002/2016JC011693.
- Mantua, N. J., S. R. Hare, Y. Zhang, J. M. Wallace, and R. C. Francis (1997), A Pacific interdecadal climate oscillation with impacts on salmon production, *Bull. Am. Meteorol. Soc.*, *78*, 1069–1079.
- Mayer, D., R. Molinari, M. Baringer, and G. Goni (2001), Transition regions and their role in the relationship between sea surface height and subsurface temperature structure in the Atlantic Ocean, *Geophys. Res. Lett.*, *28*, 3943–3946, doi:10.1029/2001GL013331.
- Meinen, C. S., S. Speich, R. C. Perez, S. Dong, A. R. Piola, S. L. Garzoli, M. Baringer, S. Gladyshev, and E. Campos (2013), Temporal variability of the Meridional Overturning Circulation at 34.5°S: Results from two pilot boundary arrays in the South Atlantic, *J. Geophys. Res. Oceans*, *118*, 6461–6478, doi:10.1002/2013JC009228.
- Morioka, Y., T. Tozuka, and T. Yamagata (2011), On the growth and decay of the subtropical dipole mode in the South Atlantic, *J. Clim.*, *24*, 5538–5554, doi:10.1175/2011JCLI4010.1.
- Nnamchi, H. C., J. Li, and R. N. C. Anyadike (2011), Does a dipole mode really exist in the South Atlantic Ocean?, *J. Geophys. Res.*, *116*, D15104, doi:10.1029/2010JD015579.
- Nnamchi, H. C., J. Li, F. Kucharski, I.-S. Kang, N. S. Keenlyside, P. Chang, and R. Farneti (2016), An equatorial-extratropical dipole structure of the Atlantic Niño, *J. Clim.*, doi:10.1175/JCLI-D-15-0894.1.
- Parker, D. E., P. D. Jones, C. K. Folland, and A. Bevan, (1994), Interdecadal changes of surface temperature since the late nineteenth century, *J. Geophys. Res.*, *99*(D7), 14,373–14,399.

- Reynolds, R. W., N. A. Rayner, T. M. Smith, D. C. Stokes, and W. Wang (2002), An improved in situ and satellite SST analysis for climate, *J. Clim.*, *15*(13), 1609–1625.
- Richter, I., S. K. Behera, Y. Masumoto, B. Taguchi, H. Sasaki, and T. Yamagata (2013), Multiple causes of interannual sea surface temperature variability in the equatorial Atlantic Ocean, *Nat. Geosci.*, *6*(1), 43–47.
- Sitz, L. E., R. Farneti, S. M. Griffies (2015), Simulated South Atlantic transport and their variability during the 1958–2007, *Ocean Model.*, *95*, 70–90.
- Smith, R. S., and J. M. Gregory (2009), A study of the sensitivity of ocean overturning circulation and climate to freshwater input in different regions of the North Atlantic, *Geophys. Res. Lett.*, *36*, L15701, doi:10.1029/2009GL038607.
- Smith, T. M., R. W. Reynolds, R. E. Livezey, and D. C. Stokes, (1996), Reconstruction of historical sea surface temperatures using empirical orthogonal functions, *J. Clim.*, *9*(6), 1403–1420.
- Stouffer, R. J., J. Yin, J. Gregory, K. Dixon, M. Spelman, W. Hurlin, A. Weaver, M. Eby, G. Flato, and H. Hasumi (2006), Investigating the causes of the response of the thermohaline circulation to past and future climate changes, *J. Clim.*, *19*(8), 1365–1387.
- Trzaska, S., A. W. Robertson, J. D. Farrara, and C. R. Mechoso (2007), South Atlantic variability arising from air-sea coupling: Local mechanisms and tropical-subtropical interactions, *J. Clim.*, *20*(14), 3345–3365, doi:10.1175/JCLI4114.1.
- Venegas, S. A., L. A. Mysak, and D. N. Straub (1997), Atmosphere–ocean coupled variability in the South Atlantic, *J. Clim.*, *10*, 2904–2920, doi:10.1175/1520-0442(1997)010<2904:AOCVIT.2.0.CO;2.
- Wang, F., and P. Chang (2008), Coupled variability and predictability in a stochastic climate model of the tropical Atlantic, *J. Clim.*, *21*(23), 6247–6259, doi:10.1175/2008JCLI2283.1.
- Yeager, S., and G. Danabasoglu (2014), The origins of late-twentieth-century variations in the large-scale North Atlantic Circulation, *J. Clim.*, *27*, 3222–3247.
- Zebiak, S. (1993), Air–sea interaction in the equatorial Atlantic region, *J. Clim.*, *6*(8), 1567–1586, doi:10.1175/1520-0442.